



ARTICLE

Activation of TRPV1 receptor facilitates myelin repair following demyelination via the regulation of microglial function

Jing-xian Sun¹, Ke-ying Zhu², Yu-meng Wang¹, Dan-jie Wang¹, Mi-zhen Zhang¹, Heela Sarlus², Irene Benito-Cuesta², Xiao-qiang Zhao¹, Zao-feng Zou^{1,3}, Qing-yang Zhong¹, Yi Feng¹, Shuai Wu⁴, Yan-qing Wang¹, Robert A. Harris² and Jun Wang¹

The transient receptor potential vanilloid 1 (TRPV1) is a non-selective cation channel that is activated by capsaicin (CAP), the main component of chili pepper. Despite studies in several neurological diseases, the role of TRPV1 in demyelinating diseases remains unknown. Herein, we reported that TRPV1 expression was increased within the corpus callosum during demyelination in a cuprizone (CPZ)-induced demyelination mouse model. TRPV1 deficiency exacerbated motor coordinative dysfunction and demyelination in CPZ-treated mice, whereas the TRPV1 agonist CAP improved the behavioral performance and facilitated remyelination. TRPV1 was predominantly expressed in Iba1⁺ microglia/macrophages in human brain sections of multiple sclerosis patients and mouse corpus callosum under demyelinating conditions. TRPV1 deficiency decreased microglial recruitment to the corpus callosum, with an associated increase in the accumulation of myelin debris. Conversely, the activation of TRPV1 by CAP enhanced the recruitment of microglia to the corpus callosum and potentiated myelin debris clearance. Using real-time live imaging we confirmed an increased phagocytic function of microglia following CAP treatment. In addition, the expression of the scavenger receptor CD36 was increased, and that of the glycolysis regulators *Hif1a* and *Hk2* was decreased. We conclude that TRPV1 is an important regulator of microglial function in the context of demyelination and may serve as a promising therapeutic target for demyelinating diseases such as multiple sclerosis.

Keywords: TRPV1; capsaicin; microglia; remyelination; phagocytosis

Acta Pharmacologica Sinica (2022) 0:1–14; <https://doi.org/10.1038/s41401-022-01000-7>

INTRODUCTION

Myelin is a lipid-rich membrane stack that wraps around large-diameter axons, and in the central nervous system (CNS), myelin is generated and maintained by oligodendrocytes (OLs) [1]. The myelin sheath is crucial for saltatory conduction, nutrition supply, axonal integrity and function [2]. Persistent demyelination leads to a variety of neurological symptoms and progressive disabilities [3]. Multiple sclerosis (MS) is an autoimmune demyelinating disorder of the CNS that is characterized by CNS inflammation, demyelination, gliosis and subsequent axonal injury [4]. The process of spontaneous remyelination following myelin injury recedes over time after relapses in MS patients, and is insufficient to prevent chronic disease for the majority of patients [5]. Remyelination is a complicated process and there are currently no therapeutic options to efficiently promote myelin regeneration. The mechanisms underlying demyelination and the potential targets for remyelination thus warrant further investigation.

Microglia are immune cells in the CNS that maintain homeostasis and become activated in response to perturbation [6], and

dysfunctional microglia are implicated in many neurological disorders. However, these cells can play both detrimental and beneficial roles in MS lesions, on the one hand, they produce inflammatory cytokines and reactivate infiltrating lymphocytes, resulting in an inflammatory loop, but conversely contributing to myelin debris removal, the secretion of regenerative factors, and the recruitment of OL precursors to sites of demyelination [7]. A recent landmark genomic study also highlighted that many risk variants of MS genes are enriched in microglia [8], suggesting that microglia are important players in the pathogenesis of MS.

Why MS is most prevalent in Nordic countries or high-latitude areas is an intriguing question that could be ascribed to genetics, environmental factors, and individual lifestyle. Certain risk factors have been identified including smoking, lack of sun exposure or low vitamin D intake, as well as Epstein-Barr virus infections [9]. Interestingly, tropical or subtropical countries such as India, Thailand, China and Mexico have a fairly low incidence of MS [4]. Apart from genetic and ethnic differences, common factors among these countries include relatively warm climates as well as

¹Department of Integrative Medicine and Neurobiology, School of Basic Medical Science, Institutes of Integrative Medicine, State Key Laboratory of Medical Neurobiology and MOE Frontiers Center for Brain Science, Institutes of Brain Science, Shanghai Medical College, Fudan University, Shanghai 200032, China; ²Department of Clinical Neuroscience, Karolinska Institutet, Center for Molecular Medicine, Karolinska University Hospital at Solna, Stockholm, Sweden; ³Department of General Surgery, Jiading Hospital of Traditional Chinese Medicine, Shanghai 201800, China and ⁴Department of Neurology, Zhongshan Hospital, Fudan University, Shanghai 200032, China

Correspondence: Robert A. Harris (robert.harris@ki.se) or Jun Wang (jwangf@shmu.edu.cn)

These authors contributed equally: Jing-xian Sun, Ke-ying Zhu, Yu-meng Wang

Received: 27 March 2022 Accepted: 12 September 2022

Published online: 13 October 2022

the use of hot and spicy food. Although a lack of sun exposure is a well-documented risk factor for MS, less is known about dietary influences.

Transient receptor potential vanilloid 1 (TRPV1), also well known as the vanilloid receptor type 1 (VR1), belongs to the transient receptor potential (TRP) channel family [10]. The receptor is a ligand-gated non-selective cationic channel that was first cloned from rat dorsal root ganglia neurons in 1997 [11]. TRPV1 can be activated by numerous physical and chemical stimuli such as high temperatures (>43 °C), low pH, capsaicin (CAP), resiniferatoxin, N-arachidonoyl-ethanolamine and ATP [12]. TRPV1 is expressed in the CNS [13–17] where it can play a major role in regulating synaptic plasticity, mediating neurological behavior and modulating neuroinflammation [18, 19]. It has been reported that mutations in the TRPV1 and cannabinoid receptor 1 (CB1) genes lead to reduced neurogenesis [20].

TRPV1 can modulate the release of different pro-inflammatory and anti-inflammatory cytokines depending on the context [21]. Induction of the experimental autoimmune encephalomyelitis (EAE) model of MS in TRPV1-deficient mice increased the mortality rate during the peak disease phase [22]. Moreover, the application of TRPV1 agonists reduced EAE disease severity [23]. These findings indicate that TRPV1 is protective in the EAE model and that TRPV1 is a potential therapeutic target for MS. However, the contribution of TRPV1 to CNS demyelinating conditions remains poorly understood. Furthermore, as the EAE model is a complicated model with a cascade of autoimmune responses involving many cell types, the underlying mechanisms through which TRPV1 is beneficial in EAE remain elusive [24].

In the present study, we used the cuprizone (CPZ)-induced demyelinating model, which directly leads to OL death and demyelination without substantial immune responses, in order to examine whether TRPV1 has a role in demyelination and remyelination processes. We determined that deletion of TRPV1 exacerbated demyelination, whereas application of capsaicin, an agonist of TRPV1, ameliorated motor coordinative dysfunction and promoted myelin recovery. We further revealed that the beneficial effects of capsaicin were associated with the modulation of microglial function.

MATERIALS AND METHODS

Animals

Adult (7–8 weeks old) male C57BL/6 mice were obtained from the Shanghai Experimental Animal Center of the Chinese Academy of Sciences. *Trpv1*^{-/-} mice (003770, Jackson Laboratory, San Mateo, California, USA) were gifted by Dr. Yuqiu Zhang (Fudan University, China). All mice were bred under standard animal room conditions. All animal experiments were performed at Fudan University and approved by the Institutional Animal Care and Use Committee of Fudan University (20180302-063).

CPZ treatment

To induce reproducible demyelination of the CNS, mice were fed a standard rodent diet containing 0.3% CPZ (Sigma) powder for 5 weeks to induce demyelination. After 5 weeks of induction, mice were kept on a standard diet for 1 week which allowed spontaneous remyelination.

Capsaicin administration

WT mice received different doses of capsaicin (1, 2, and 5 mg/kg of body weight, MCE) by intraperitoneal injection every other day for 2 weeks. *Trpv1*^{-/-} mice were intraperitoneally injected with 2 mg/kg of CAP every other day for 2 weeks.

Beam walking test

The beam walking test was performed as previously described [25]. The apparatus consisted of a narrow wood beam and a safety

box. Mice were trained to walk toward a safety box on a 1-meter-long wooden beam before testing. The time required for passing through the beam over two repeats was recorded. The average of two trials was used for analysis. The cut-off value was set at the 20 s.

Accelerating rotarod test

Motor performance was estimated by accelerating the rotarod test. Each group of animals was placed on an accelerating rotarod (Columbus Instruments) walking for 300 s from 4 to 40 rpm. Latency was automatically recorded from the beginning of the trial until the mouse falls off. The rotarod latency was collected three times with a 30-min interval between each test, then an average of three trials was calculated.

Immunohistochemistry

Mice were anesthetized with the injection of pentobarbital sodium (70 mg/kg body weight) and perfused with saline followed by 4% PFA. Brain tissues were dissected into 20 μm sections. Before staining, sections were washed three times in PBS and blocked for 60 min at room temperature with 4% goat serum in 0.3% Triton X-100. Then the brain sections were incubated with rabbit anti-MBP (ab40390, 1:400, Abcam), mouse anti-CC1 (OP80, 1:200, Millipore), rabbit anti-Iba1 (019-19741, 1:400, Wako), rabbit anti-dMBP (ab5864, 1:500, Millipore), mouse anti-VR1 (ab203103, 1:200, Abcam), rabbit anti-Olig2 (AB9610, 1:300, Millipore), rabbit anti-GFAP (80788, 1:800, CST), rabbit anti-NeuN (ab177487 1:200, abcam) overnight at 4 °C. After washing with PBS three times, primary antibodies were visualized with Alexa 488-conjugated and 594-conjugated secondary antibodies (1: 1000, Invitrogen) for 2 h at room temperature. Compact myelin staining was performed with FluoroMyelin Green Fluorescent (F-34651, Invitrogen) according to the manufacturer's instructions. For the CC1 and FluoroMyelin staining, images were captured by a fluorescence microscope (Leica). All the other images were captured by laser confocal scanning fluorescence microscope (Olympus/Nikon).

Human brain section staining

Human brain samples were obtained from the Netherlands Brain Bank in Amsterdam (coordinator Dr. I. Huitinga) with the kind help of Dr. Sandra Amor. Brain tissues from MS patients were diagnosed according to the McDonald criteria [26]. Healthy controls refer to age-matched controls without neurological conditions. Participants or close family members were informed and consented to brain autopsy and the use of tissues for research purposes. Tissues were fixed in 4% paraformaldehyde, processed and paraffin-embedded. MS brain sections were determined and classified based on the size and type of lesion for quantitative analyses. Identification of the lesions was acquired by immunohistochemistry for myelin proteolipid protein to detect myelin loss and HLA-DR to detect myeloid cell activation. Human brain sections were deparaffined and stained with anti-TRPV1 antibody (NB300-122, 1:500, Novus) and anti-Iba1 antibody (019-19741, 1:500, WAKO).

Western blot analysis

Corpus callosum (CC) tissues were collected on ice in RIPA buffer containing PMSF. Protein levels in the lysates were quantified by Pierce bicinchoninic acid Protein Assay Kit (23225, Thermo) and adjusted equally. Samples were separated by SDS-PAGE (10%) gels and transferred to PVDF membranes (Merck Millipore). Membranes were blocked with 5% BSA and then incubated with primary antibodies recognizing TRPV1 (ab203103, 1:500, Abcam), TRPV1 (sc-398417, 1:500, Santa Cruz Biotechnology), MBP (ab40390, 1:1000, Abcam) and β-actin (60004, 1: 10,000, Proteintech). After incubation with secondary HRP-labeled antibodies (Proteintech), protein bands were detected by the ECL chemiluminescence detection system. Imaging of bands was performed

Table 1. The sequences of primers used in the study.

Gene	Primer forward (5'-3')	Primer reverse (5'-3')
<i>Gapdh</i>	AAATGGTGAAGGTCGGTGTG	AGGTCAATGAAGGGGTCGTT
<i>Hprt</i>	AGTG TTGATACAGGCCAGAC	CGTGATTCAAATCCCTGAAGT
<i>Mbp</i>	AAGTACCTGGCCACAGCAAG	AGCTTCTCTACGGCTCGGA
<i>Cnp</i>	AGAGTGATCCTTGGAGCCAGA	CGGAGGGGAATGGTGGATTT
<i>Mag</i>	TCTCTACCCGGGATTGCTACT	CGGATTCTGCATACTCAGCCA
<i>Plp1</i>	CTGAGCGCAACGTTTGTGG	TACATTCTGGCATCAGCGCA
<i>Pdgfra</i>	GGAGACTCAAGTAACCTTGAC	TCAGTTCTGACGTTGCTTCAA
<i>Sox10</i>	AGGTTGCTGAACGAAAGTGAC	CGTGACGAGGACACAGTC
<i>Olig2</i>	TCCCAGAACCCGATGATCTT	CGTGACGAGGACACAGTC
<i>Olig1</i>	TCTCCACCGCATCCCTTCT	CCGAGTAGGGTAGGATAACTCTG
<i>Hif1a</i>	CCTGCACTGAATCAAGAGGTGC	CCATCAGAAGGACTTGCTGGCT
<i>Hk2</i>	GGAGAGCACGTGTGACGAC	GATGCGACAGGCCACAGCA
<i>Cd36</i>	ATGGGCTGTGATCGGAACTG	GTCTTCCAATAAGCATGTCTCC
<i>Nos2</i>	TCCAGAATCCCTGGACAAGCTGC	TGCAAGTGAATCCGATGTGGCCT

with an Image-Quant LAS4000 mini image analyzer (GE Healthcare). The bands of Western blot were analyzed using Quantity One software. The quantitative statistical graphs were created based on the relative fold change.

Oil Red O staining

For the preparation of frozen sections, the mice were perfused with 4% PFA, and brain tissue was cut into 25 µm sections. The slices were washed in distilled water and subsequently rinsed in 60% isopropyl alcohol for 2 min. Then the slices were incubated with Oil Red O solution at 60 °C for 15 min. Sections were stained with hematoxylin within 1 min followed by a step of hydrochloric acid alcohol differentiation for 5 s.

Reverse transcription-polymerase chain reaction (RT-PCR) analysis Tissues and cells were lysed in RLT buffer and RNA was extracted using the RNeasy mini kit (74106, Qiagen) in the automated QIAcube (Qiagen) following the provided instructions. On-column DNase digestion was performed using the RNase-Free DNase Set (79254, Qiagen). Reverse transcription of total RNA was performed using the iScript cDNA Synthesis Kit (1708891, Bio-Rad) after RNA extraction. Complementary DNA was stored at -20 °C until use. Quantitative polymerase chain reaction (qPCR) was performed in duplicates using a CFX38 Real-Time PCR Detection Systems with SYBR green as fluorophore (Bio-Rad). Target expression was calculated using the Bio-Rad CFX Manager V1.6. software. *Hprt*, *Gapdh*, or the geometrical mean of two of those was used as housekeeping gene reference. Primer sequences used in this study are listed in Table 1.

Electron microscopy

Mice brain tissues for electron microscopy were sliced at a thickness of 1 mm and postfixed in TEM fixation solution at 4 °C. The samples were dehydrated through alcohols and embedded in acetone and embedding medium (Servicebio) following standard procedures. Ultra-thin sections were cut by an ultramicrotome (Leica UC7) and imaged using a FEI TECNAI G2 20 TWIN electron microscope.

Primary microglia culture and BV2 microglial cells culture

For migration and wound scratch assays (performed at Fudan University): primary mixed glia was isolated from the cortices of neonatal Sprague–Dawley rats (P0-1) as previously described without discriminating by sex. Mixed glial cells were maintained in T75 flasks for 12 days in DMEM/F12 medium (HyClone), containing

10% FBS (Gibco), and 20 ng/mL m-CSF (R&D Systems). At 13 days after plating, the flasks were shaken on an orbital shaker for 2 h at 200 r/min to collect microglial cells. For the phagocytosis assay, microglia are isolated from adult C57BL/6Ntac mice. Mice were euthanized with an overdose of pentobarbital sodium and perfused with ice-cold PBS. The dissected brains were transferred to a 15 mL tube containing 5 mL enzymatic solution composed of papain (Worthington; 1:100 dilution in L15 medium) and filtered using a 0.2 µm cell strainer. The brain was dissociated in the enzymatic solution through gentle pipetting followed by incubation at a 37 °C water bath for 10 min, followed by physical dissociation by pipetting until no big tissue chunk was visible. In total, 20 µL of 0.2 mg/ml DNase I (Roche) was added to the tube, followed by another 10 min incubation. After thorough dissociation, the enzymatic reaction was stopped by adding ice-cold HBSS, and the solution was transferred to a 50 mL tube passing through a 40 µm cell strainer. Cell pellets were collected by centrifuging at 300 × g, 5 min, 4 °C, resuspended in 20 mL 38% isotonic Percoll (7.6 mL stocking Percoll, 0.84 mL 10× HBSS, and 11.56 mL 1× HBSS) and centrifuged at 800 × g (4 acceleration, no brake) for 10 min, at room temperature. The floating myelin layer was removed after centrifugation, and the pellets were washed once with cold HBSS. Cells were then resuspended and cultured in DMEM/F12 complete medium with 10% FBS, 100 units/mL Penicillin and 100 µg/mL Streptomycin (Sigma-Aldrich) and 20 ng/ml m-CSF. The medium was changed twice a week, and after 14 days, the microglia were separated from the mixed culture by magnetic MicroBeads (130-049-601, Miltenyi Biotec) attached to an anti-CD11b antibody following the manufacturer's protocol. For the culture of BV2 microglia, cells were cultured in the same medium as adult primary microglia, but without the supplement of m-CSF.

Cell survival

Cell viability was determined by CellTiter-Glo Luminescent Cell Viability Assay (Promega, G7571). Primary microglial cells were plated in a 96-well plate at a concentration of 3000 cells per well in 100 µL medium. In total, 100 µL CellTiter-Glo reagent was added to each well. After 10 min of incubation at room temperature, luminescence was measured to indicate ATP levels in live cells by a microplate reader. The average luminescence of the controls was taken as 100%.

Transwell migration assay

To investigate the role of TRPV1 on migration, isolated microglial cells in DMEM/F12 with 0.5% FBS were plated in the upper

compartment of the Boyden chamber (8 μm pore size) in the presence of CAP and/or CPZ at the indicated concentrations. CAP and CPZ were purchased from MCE. The cells were allowed to migrate for 24 h to the lower compartment containing 600 μL DMEM/F12 with 5% FBS. After 24 h of incubation, the membranes were fixed and stained with DAPI. Images were captured under an inverted fluorescence microscope (Olympus). The number of migrated cells was quantified by counting five random distinct fields under a microscope. The number of migrated control cells was taken as 100%.

Scratch-wound assay

To assay the migration capability of microglia, BV2 cells were seeded into a 6-well plate. A wound was created by scratching with a 1000 μL sterile pipette tip. Scratched BV2 cells were washed with PBS and then maintained in a culture medium with low serum. Cells were imaged 24 h after scratching under an inverted microscope.

Flow cytometry

Cells were incubated with 4 mM ethylenediaminetetraacetic acid for 30 min at 37 °C to detach, followed by physical pipetting with PBS on ice. The detached cells were first stained with the LIVE/DEAD Fixable Yellow Dead Cell Stain Kit (L34959, Invitrogen) to remove dead cells. For quantification of dextran uptake: cultured primary microglia were incubated with Alexa Fluor 488-conjugated dextran (1 μg/ml; D22910, Invitrogen) in a 37 °C incubator for 30 min, followed by a rinse with warm PBS and staining with A700 anti-mouse CX3CR1 antibody (1:200 dilution; clone: SA011F11, 149036, BioLegend). For quantification of CD36 expression: BV2 microglia were incubated with PE anti-mouse CD36 antibody (1:200; clone: HM36, 102605, BioLegend). The cells were then acquired using a FACVerse flow cytometer (BD Biosciences) and the data were analyzed using Flowjo or Kaluza.

siRNA transfection

Primary microglia or BV2 microglial cells were incubated with 30 nM SMARTPool ON-TARGETplus siRNA-TRPV1 (L-066223-00-0005, Horizon Discovery) or ON-TARGETplus Non-targeting Control Pool (D-001810-10-05, Horizon Discovery) mixed with Lipofectamine RNAiMAX Transfection Reagent (13778030, Invitrogen) in Opti-MEM I Reduced Serum Medium (31985062, Gibco) according to the manufacturer's protocol. After 24 h, the medium was removed and washed with warm PBS.

IncuCyte live-cell imaging of phagocytosis

Primary microglia were cultured in an IncuCyte ImageLock 96-well plate (Essen BioSciences) at a density of 15,000–20,000 cells per well. The cells were incubated with capsaicin for 12 h or siRNA-TRPV1 for 24 h in a serum-free, m-CSF-free medium, and the medium was changed to a serum-free, m-CSF-free medium containing 0.1 mg/mL pHrodo Red Zymosan Bioparticles (P35364, Invitrogen). The plates were put into an IncuCyte ZOOM live-cell analysis system and analyzed with IncuCyte Zoom software (2018A) following the analysis protocols provided by the manufacturer.

Statistics

All statistical data in the figures are expressed as mean values ± standard error of the mean. Statistical analyses and graphs were performed using GraphPad Prism 8 software. Statistical tests used to calculate *P* values are described in the respective figure legends. For all data, *P* values <0.05 were considered statistically significant.

RESULTS

TRPV1 deficiency exacerbates demyelination

To induce demyelination in the CNS we employed a CPZ-induced demyelinating model by feeding mice with chow containing CPZ.

After 5 weeks, CPZ was removed from the diet to allow spontaneous repair, and we evaluated demyelination at the end of week 6 (Fig. 1a). We first quantified the protein expression of TRPV1 in the CC, as this is the most highly myelinated region in the brain. We recorded an increased expression of TRPV1 in the CC after a 5-week CPZ administration (Fig. 1b, c), indicating a strong correlation between TRPV1 expression and demyelination.

This finding prompted us to further determine the role of TRPV1 in demyelinating conditions by inducing demyelination in both wild-type (WT) mice and *Trpv1*^{-/-} mice. Significant body weight loss was observed in all mice following CPZ administration, without a significant difference between the two genotypes (Fig. 1d). Beam walking and rotarod tests were used to assess the motor coordinative function of mice, which is affected by CPZ-induced demyelination [25]. The absence of TRPV1 did not affect the motor coordinative function under naive conditions, while in *Trpv1*^{-/-} mice a more severe locomotor impairment was observed after 6 weeks of CPZ treatment (Fig. 1e).

The degree of myelination can be assessed by measuring the levels of myelin basic protein (MBP). Western blotting revealed that the protein levels of MBP in the CC was significantly decreased in *Trpv1*^{-/-} mice compared to that in WT mice (Fig. 1f, g). This finding was further confirmed by immunofluorescent staining of MBP in the CC region (Fig. 1h). We used transmission electron microscopy (TEM) to further evaluate the myelin microstructure. Both the WT and *Trpv1*^{-/-} mice exhibited significant decreases in myelinated axons after CPZ treatment. Notably, there was a remarkable decrease in myelinated axons in the CC of *Trpv1*^{-/-} mice compared to that of the WT mice after CPZ treatment (Fig. 1i, j). Taken together, these data demonstrate that TRPV1 deficiency exacerbates CPZ-induced demyelination.

Activation of TRPV1 by capsaicin improves myelination

Since TRPV1 deletion had a detrimental outcome in CPZ-induced demyelination, we next examined whether an enforced gain-of-function of TRPV1 would have a beneficial effect on demyelination. We selected capsaicin, an agonist of TRPV1, to activate TRPV1 in these experiments. WT mice were intraperitoneally injected with vehicle or different doses of capsaicin for 2 weeks. Treatment with 2 mg/kg capsaicin significantly ameliorated the outcomes of both the beam walking and rotarod tests (Fig. 2b), and we selected 2 mg/kg capsaicin (hereafter referred to as the CAP groups) for all subsequent experiments. We also administered CAP to naive mice to evaluate whether CAP could alter motor coordinative function, and we showed that CAP treatment per se did not alter any phenotype in WT mice (Supplementary Fig. 1).

RT-PCR analysis revealed an increase in myelin genes or the genes of mature OLS after CAP treatment, but the expression of OPC/OL lineage genes remained unchanged (Fig. 2c). We then performed immunofluorescence analysis of CC1 (mature OLS), and found that CAP treatment increased OL numbers in the CC. Compared to WT mice, *Trpv1*^{-/-} CPZ mice showed a decreased number of CC1⁺ cells in the CC (Fig. 2d, e). CAP treatment also increased the protein level of MBP in the CC of WT mice (Fig. 2f–h) and TEM analysis revealed that CAP treatment increased the number of myelinated axons (Fig. 2i, j). However, this ameliorative effect was not evident when CAP was administered to *Trpv1*^{-/-} mice (Fig. 2k). These data demonstrate that activating TRPV1 with CAP protects against CPZ-induced demyelination and promotes subsequent remyelination.

TRPV1 is expressed on microglia under demyelinating conditions. While previous studies showed that TRPV1 was mainly distributed in neuronal cell bodies in many brain regions [27], the cellular distribution of TRPV1 in the CNS is not fully characterized, especially during demyelination, and both microglia and astrocytes are also reported to express TRPV1 [28, 29]. We used double immunostaining to observe the localization of TRPV1 in the CC of

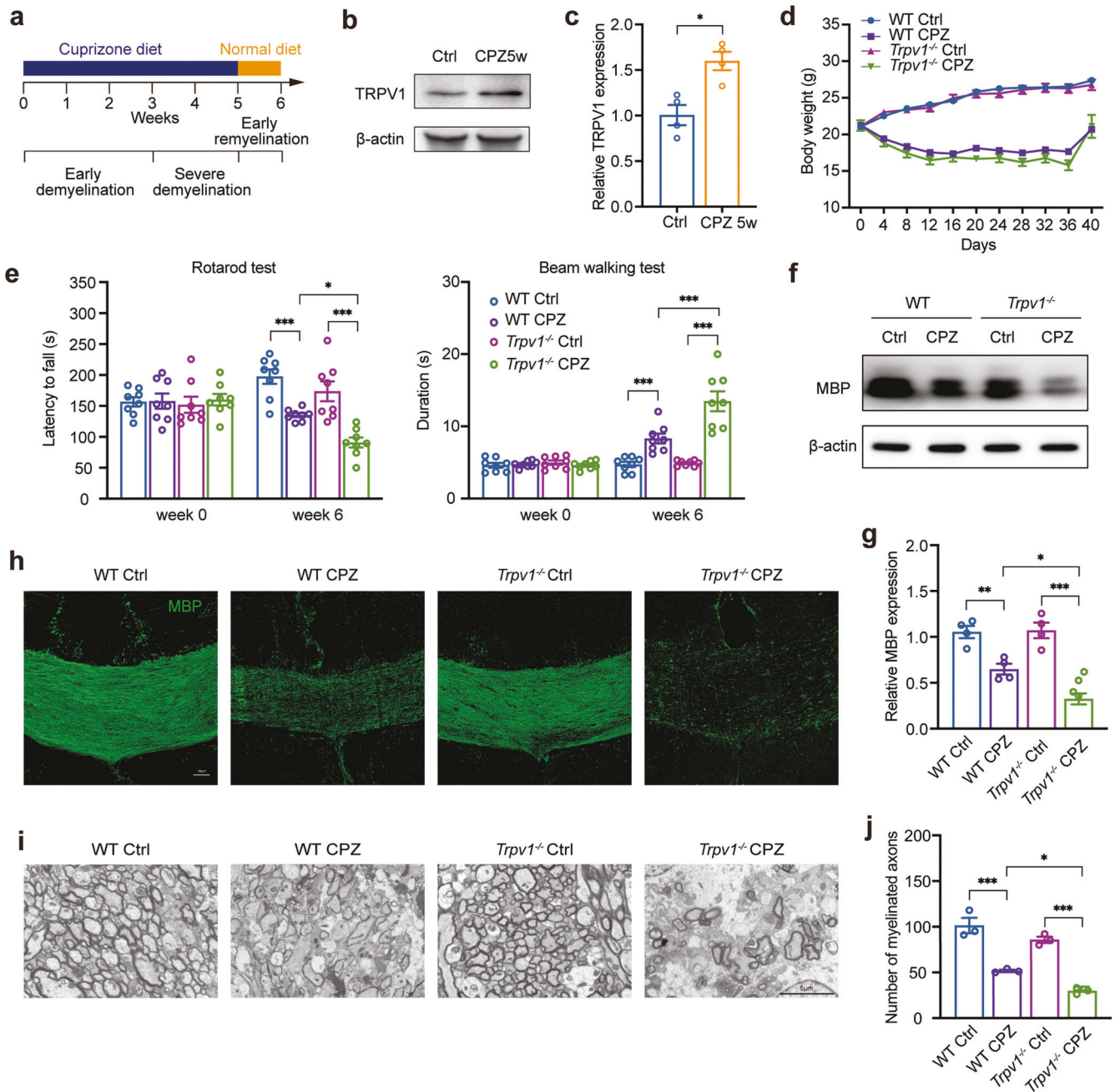


Fig. 1 TRPV1 deficiency exacerbates motor coordinative dysfunction and demyelination. **a** Experimental schematic of the cuprizone (CPZ)-induced demyelinating model. **b** The expression of TRPV1 protein in the corpus callosum of control or CPZ-treated mice was assessed by Western blotting and normalized with β -actin expression. **c** The quantification of TRPV1 expression (mean \pm SEM; $n = 4$ mice for each group; * $P < 0.05$ by unpaired two-tailed *t*-test) in **b**. **d** Body weight change of WT and TRPV1 KO mice after CPZ treatment over time ($n = 8$ mice for each group; statistics performed using two-way ANOVA with Tukey's multiple comparisons test). **e** Motor coordinative function was assessed by rotarod test and beam walking test (mean \pm SEM; $n = 8$ mice for each group; * $P < 0.05$, *** $P < 0.001$ by two-way ANOVA with Tukey's multiple comparisons test). **f** The expression of MBP protein was assessed using Western blotting and normalized with β -actin expression. **g** The quantification of MBP expression (mean \pm SEM; $n = 4$ mice for each group; * $P < 0.05$, ** $P < 0.01$, *** $P < 0.001$ by two-way ANOVA with Sidak's multiple comparisons test) in **f**. **h** Representative immunofluorescent images of MBP staining in the corpus callosum (scale bar = 50 μ m). **i** Representative TEM images showing the ultrastructure of myelin/axons in the corpus callosum (scale bar = 5 μ m). **j** Quantification of myelinated axons (mean \pm SEM; $n = 3$ randomly selected areas from one sample of each group; * $P < 0.05$, *** $P < 0.001$ by two-way ANOVA with Tukey's multiple comparisons test) in **i**.

adult mice under both naïve conditions and CPZ-induced demyelinating conditions, and determined that the majority of Iba1⁺ cells expressed TRPV1 (Fig. 3a, b and Supplementary Fig. 2). Furthermore, we investigated whether TRPV1 was expressed in human microglia. We included brain sections from healthy donors, and normal-appearing white matter (NAWM) and active lesion

areas from MS patients. Iba1 was used to label microglia and infiltrating macrophages. We observed that human microglia also expressed TRPV1. In the brain sections of healthy donors, there was very little Iba1-positive staining. By contrast, in the NAWM and active lesion areas of MS patients, Iba1 immunoreactivity was strong. In addition, the Iba1⁺ cells in the active lesion area were

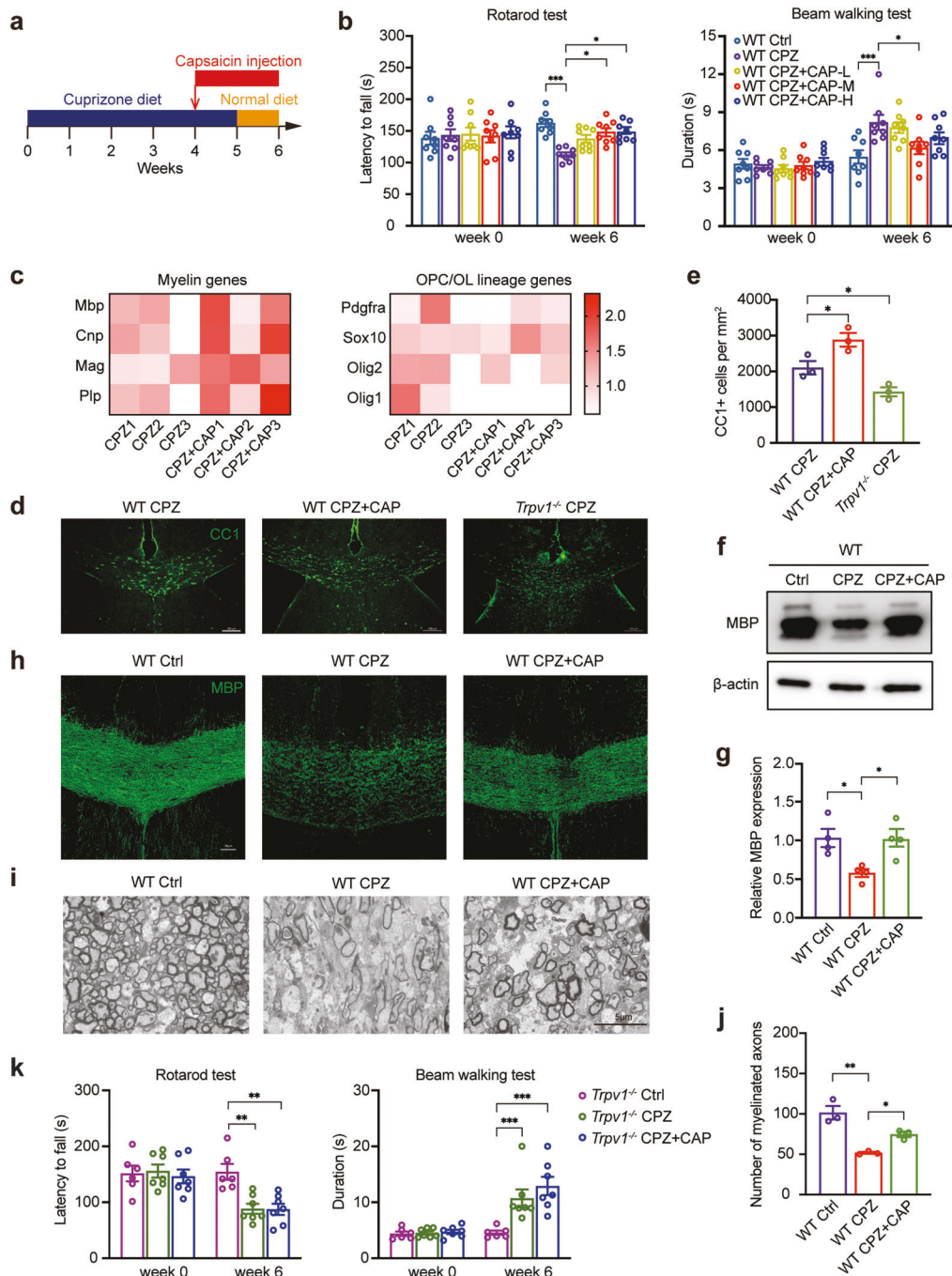


Fig. 2 Activation of TRPV1 enhances remyelination. **a** Scheme of capsaicin treatment in the CPZ-induced model. **b** Rotarod test and beam walking test graphs demonstrate the motor coordinative function of WT mice treated with different doses of capsaicin: CAP-L, CAP-M, and CAP-H represent 1 mg/kg, 2 mg/kg, and 5 mg/kg of capsaicin i.p injection, respectively (mean \pm SEM; $n = 8$ mice for each group; $*P < 0.05$, $***P < 0.001$ by two-way ANOVA with Sidak's multiple comparisons test). **c** The mRNA expression of genes related to mature oligodendrocyte/myelin (left panel) or oligodendrocyte lineage (right panel) was analyzed using RT-PCR; the color represents the value of the relative expression of a gene in a sample compared to the average value of this gene expression of the CPZ group; bright red represents a higher value, whereas a lower value is close to white color (mean \pm SEM; $n = 3$ mice for each group). **d** Representative immunofluorescent images of mature oligodendrocytes (CC1⁺) in the corpus callosum. **e** Quantification of CC1⁺ mature oligodendrocytes (mean \pm SEM; $n = 3$ mice for each group, scale bar = 100 μ m, WT CPZ + CAP vs. WT CPZ, *Trpv1*^{-/-} CPZ vs. WT CPZ, $*P < 0.05$ by unpaired two-tailed *t*-test) in **d**. **f** Western blotting analysis of MBP protein expression (normalized with β -actin expression) in the corpus callosum at the end of capsaicin treatment. **g** The quantification of MBP expression (mean \pm SEM; $n = 4$ mice for each group; $*P < 0.05$ by one-way ANOVA with Tukey's multiple comparisons test) in **f**. **h** Representative immunofluorescent images of MBP staining in the corpus callosum (scale bar = 50 μ m). **i** Representative TEM images showing the ultrastructure of myelin/axons in the corpus callosum (scale bar = 5 μ m). **j** Quantification of myelinated axons (mean \pm SEM; $n = 3$ randomly selected areas from one sample of each group; $*P < 0.05$, $**P < 0.01$ by one-way ANOVA with Tukey's multiple comparisons test) in **i**. **k** Motor coordinative function of *Trpv1*^{-/-} mice treated with 2 mg/kg capsaicin was analyzed by rotarod test and beam walking test; (mean \pm SEM; $n = 6-7$ mice for each group; $**P < 0.01$, $***P < 0.001$ by two-way ANOVA with Tukey's multiple comparisons test).

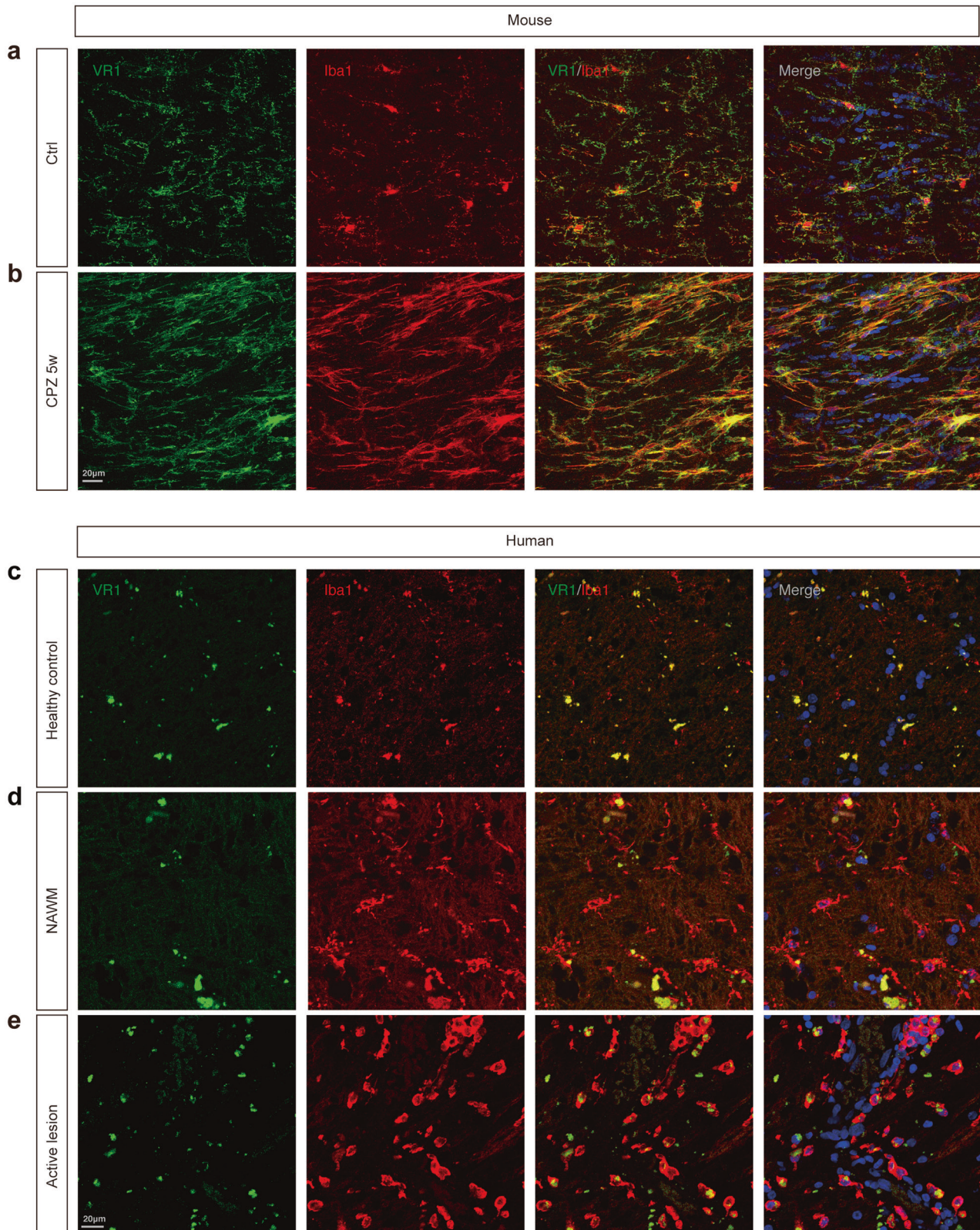


Fig. 3 TRPV1 is predominantly expressed in microglia in the homeostatic and demyelinating CNS. **a, b** Double immunostaining of VR1 (green) and Iba1 (red) in the corpus callosum of adult mice. Scale bar = 20 μm. **c–e** Double immunostaining of VR1 (green) and Iba1 (red) in healthy control, MS patients' normal-appearing white matter (NAWM) and active lesions. Scale bar = 20 μm.

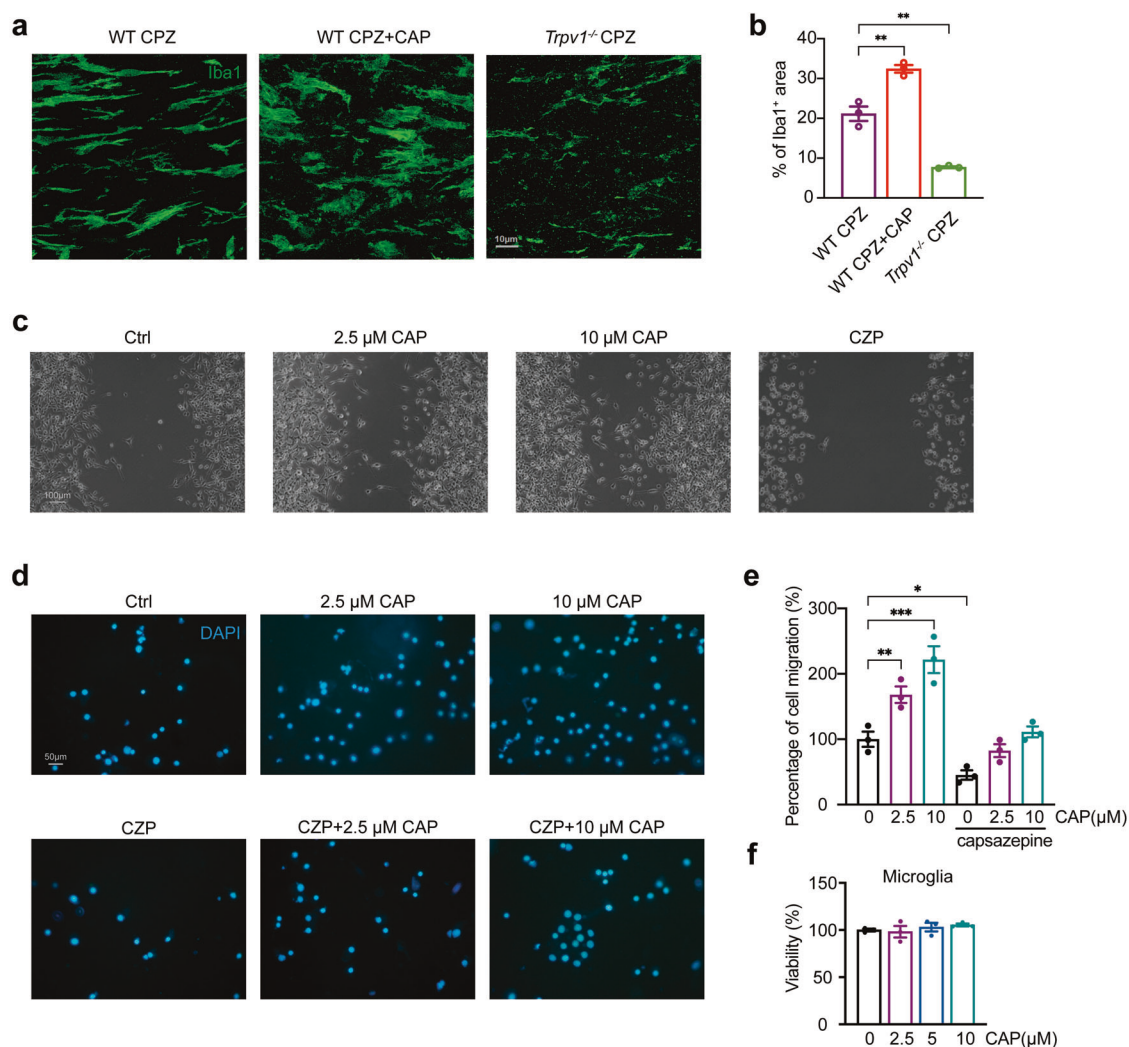


Fig. 4 TRPV1 modulates the migration of microglia. **a** Representative immunofluorescent images of Iba1 staining showing the microglial cell density in the corpus callosum; scale bar = 10 μm. **b** The statistics of **a** comparing the percentage of Iba1⁺ area per field in the corpus callosum (mean ± SEM; *n* = 3 mice for each group; WT cuprizone (CPZ) + CAP vs. WT CPZ, *Trpv1*^{-/-} CPZ vs. WT CPZ, ***P* < 0.01 by unpaired two-tailed *t*-test. **c** Representative images showing the wound scratch assay of BV2 microglial cells treated with capsaicin or capsazepine after 24 h; scale bar = 100 μm. **d** Isolated primary microglia were cultured in a transwell system, and cells in the lower compartment were stained with DAPI (CAP: capsaicin, CZP: 10 μM capsazepine treatment); scale bar = 50 μm. **e** Quantification of the percentage of microglial migration exposed to capsaicin or/and capsazepine from the transwell experiment (mean ± SEM; the number of migrated cells was quantified by counting five random fields; *n* = 3 wells; **P* < 0.05, ***P* < 0.01, ****P* < 0.001 by one-way ANOVA with Dunnett's multiple comparisons test). **f** Viability of primary microglia at 24 h after capsaicin treatment (mean ± SEM; *n* = 3 wells; statistics performed using one-way ANOVA with Tukey's multiple comparisons test).

more amoeboid and round than cells in the NAWM, which were more ramified and branched. Interestingly, we noted that in the human brain sections, TRPV1 was more abundant in round Iba1⁺ microglia/macrophages in the active lesion areas of MS patients (Fig. 3c–e). Since mounting evidence indicates that microglia play a pivotal role in the regulation of demyelination and remyelination [30], these results led us to reason that microglial TRPV1 may regulate myelination under demyelinating conditions and mediate CAP-induced promotion of remyelination.

TRPV1 regulates microglial migration

After CPZ-induced demyelination, sufficient microglial recruitment is indispensable for efficient clearance of myelin debris and subsequent remyelination [31]. We determined that CAP treatment greatly increased the number of microglia in the CC of WT mice as evidenced by increased Iba1 immunostaining. In contrast, *Trpv1*^{-/-} mice had a significantly decreased number of microglia in the CC after CPZ treatment (Fig. 4a, b). This finding

indicates that microglial recruitment or proliferation might be affected in the absence of TRPV1. To verify this hypothesis, we first used a transwell system to evaluate the effect of TRPV1 on the chemotactic activity of microglia, and the number of DAPI⁺ cells in the lower compartment of the transwell represented migrated cells. We found that CAP increased the migration of microglia to the lower transwell compartment in a concentration-dependent manner. Likewise, treatment with the TRPV1 inhibitor capsazepine (CZP) induced a significant decrease in the number of DAPI⁺ counts, and abolished the migratory effect of CAP (Fig. 4d, e). Notably, CAP treatment did not affect the viability of microglia (Fig. 4f). We also confirmed these findings using a scratch-wound assay and the BV2 microglial cell line. CAP-treated BV2 microglia had increased migration and enhanced confluence over the scratched area, whereas CZP hindered motility and reduced BV2 migration (Fig. 4c). These results indicate that the activation of TRPV1 facilitates the migration and motility of microglia.

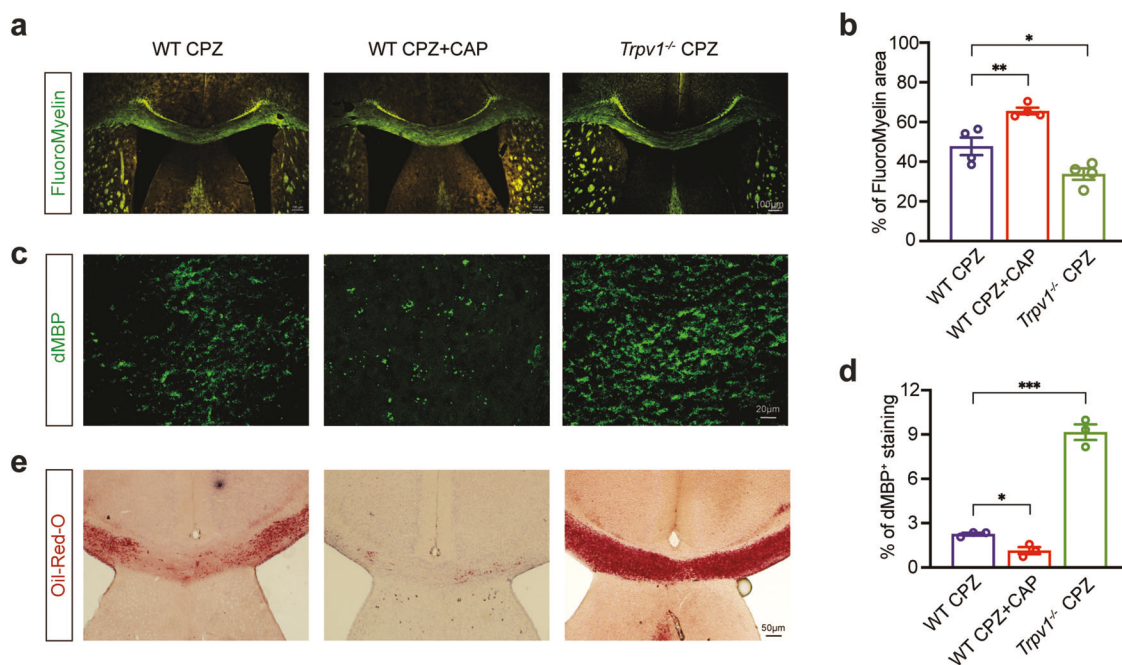


Fig. 5 TRPV1 function determines the clearance of myelin debris following demyelination. **a** Representative images for compact myelin by FluoroMyelin staining, scale bar = 100 μ m. **b** Quantification of FluoroMyelin staining in the corpus callosum (mean \pm SEM; $n = 4$ mice for each group; WT CPZ + CAP vs. WT CPZ, *Trpv1*^{-/-} CPZ vs. WT CPZ, * $P < 0.05$, ** $P < 0.01$ by unpaired two-tailed *t*-test). **c** Myelin debris in the corpus callosum was assessed by immunostaining using a specific antibody to label degraded myelin basic protein (dMBP); scale bar = 20 μ m. **d** Quantification of dMBP positive staining in the corpus callosum (mean \pm SEM; $n = 3$ mice for each group; WT CPZ + CAP vs. WT CPZ, *Trpv1*^{-/-} CPZ vs. WT CPZ, * $P < 0.05$, *** $P < 0.001$ by unpaired two-tailed *t*-test). **e** Myelin debris was detected using Oil Red O staining and presented as red lipid droplet; scale bar = 50 μ m.

Enhanced clearance of myelin debris and phagocytosis of microglia following TRPV1 activation

The efficient clearance of myelin debris, which is mainly performed by microglia, is crucial for remyelination to occur and for the restoration of myelin integrity [32]. Here, we used FluoroMyelin to evaluate myelin integrity, and noted that CAP treatment enhanced myelin integrity in the CC of CPZ-treated mice, whereas *Trpv1*^{-/-} mice showed worsened myelin integrity compared to WT mice (Fig. 5a, b). We examined the degree of fragmented myelin by using dMBP, a specific antibody that detects myelin debris. As expected, the activation of TRPV1 by CAP improved the clearance of myelin debris in the CC in WT mice. Conversely, we observed greater accumulation of degraded myelin after CPZ administration in *Trpv1*^{-/-} mice than in WT mice (Fig. 5c, d). As myelin debris is accumulated as a lipid-rich deposit, we also visualized and evaluated the amount of myelin debris using Oil Red O staining. Compared to WT mice, *Trpv1*^{-/-} mice had a larger Oil Red O⁺ area in the CC, and CAP administration of WT mice reduced the extent of the Oil Red O⁺ areas (Fig. 5e).

Whether TRPV1 activation affects the phagocytic function of microglia is not fully elucidated. Given that TRPV1 regulates the clearance of myelin debris, we hypothesized that TRPV1 also regulates the phagocytic ability of microglia. We first analyzed dextran uptake of cultured adult primary microglia by flow cytometry, including IL-4 stimulated microglia as a positive control group. We noted an increased uptake of Alexa 488-conjugated dextran in CAP-treated microglia, indicating enhanced endocytosis (Fig. 6a, b). Since the diameter of dextran is usually less than 10 nm, we then used pHrodo Red-conjugated Zymosan bioparticles with a diameter of 2–3 μ m for analysis [33]. The pH-sensitive pHrodo Red-conjugated Zymosan is non-fluorescent outside the cell but fluorescence brightly red as the lysosomal pH value is lower than the extracellular pH value due to lower concentrations of HCO₃⁻. We employed a real-time live-cell imaging system

(IncuCyte) to assess Zymosan phagocytosis by microglia over time and confirmed a dose-dependent enhancement of phagocytosis in response to CAP (Fig. 6c, d). To further confirm the involvement of TRPV1 in microglial phagocytosis, we transfected microglia with siRNA to reduce TRPV1 expression (Fig. 6e, f). We confirmed a reduced Zymosan uptake when TRPV1 was downregulated (Fig. 6h–j), which was further validated by immunocytofluorescent staining (Fig. 6g, k). Taken together, these results confirm an enhanced phagocytic ability of microglia following TRPV1 activation.

The scavenger receptor CD36 is upregulated following TRPV1 activation

We next wondered which receptors mediate the phagocytic function of microglia following capsaicin treatment. Receptors that are predominantly expressed by myeloid cells, such as TREM2 and CD36 are well-documented receptors involved in the phagocytic function of microglia [34]. We therefore analyzed the expression of these receptors following CAP treatment. While there was no detectable change in the mRNA expression of *Trem2* (data not included), we noted a significant increase in the mRNA expression of *Cd36* in bone marrow-derived macrophages treated with capsaicin (Supplementary Fig. 3). A similar increased *Cd36* expression was also evident in resting and LPS/IFN- γ -stimulated primary microglial cells after 4 h of incubation with CAP (Fig. 7a). In contrast, TRPV1 knockdown using siRNA decreased *Cd36* expression (Fig. 7b). We further characterized the protein expression of CD36 using flow cytometry and also confirmed an elevated CD36 expression in microglia treated with CAP for 24 h (Fig. 7c, e). As expected, the expression of CD36 correlated with the level of dextran uptake (Supplementary Fig. 4).

STRING analysis revealed a close protein-protein interaction between TRPV1 and CD36; with the nuclear receptor peroxisome proliferator-activated receptor γ (PPAR γ) has been reported to link the interaction in *Homo sapiens* and the proto-oncogene tyrosine-

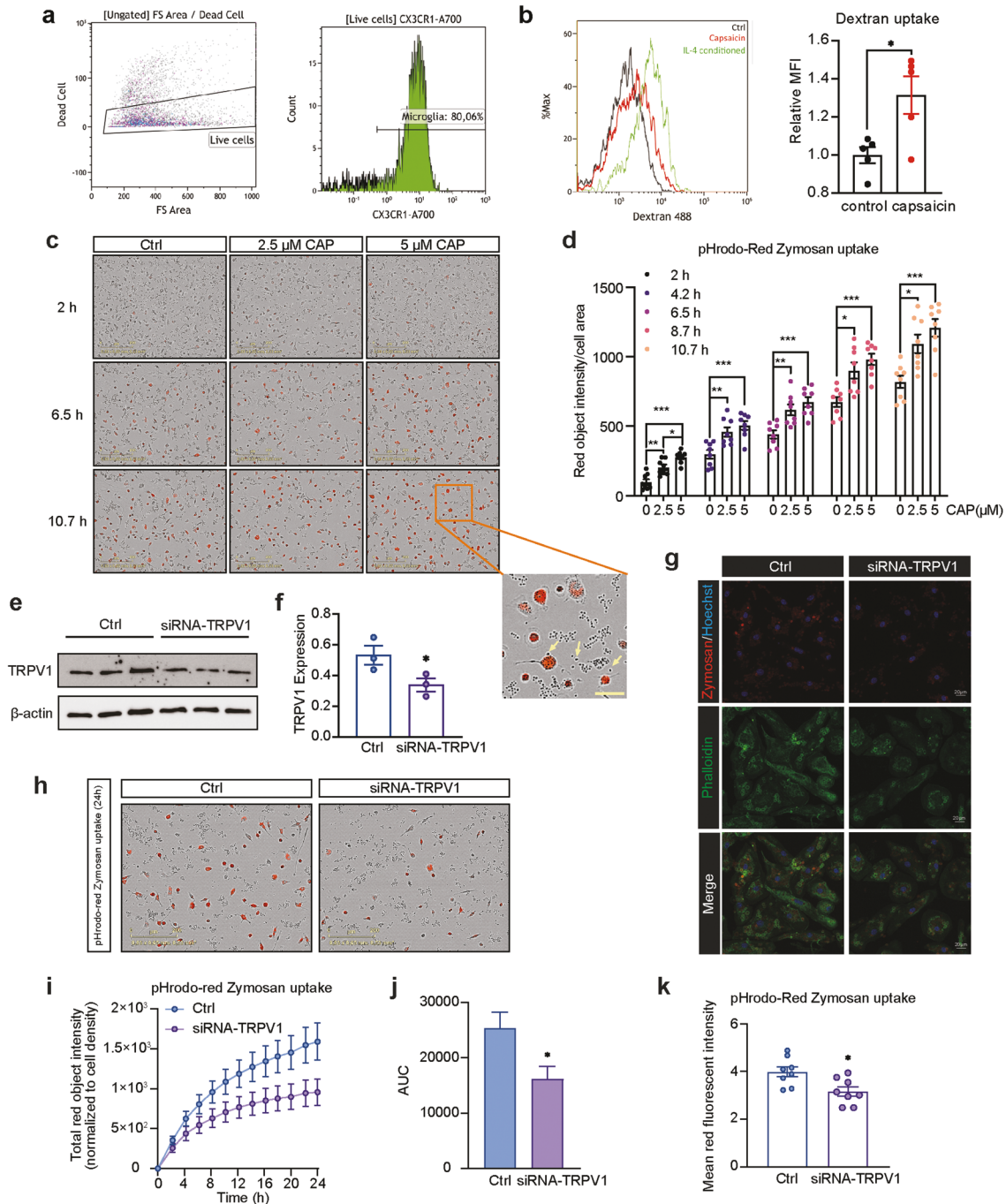


Fig. 6 TRPV1 regulates microglial phagocytosis. **a** Cultured primary microglia were treated under indicated conditions overnight and analyzed using flow cytometry with the removal of dead cells. **b** Left panel: an overlay of the histogram of the 488 signal, indicative of the uptake of dextran beads. Green: IL-4 treated cells (as a positive control group); red: capsaicin-treated cells; black: untreated naïve condition. Right panel: the median fluorescent intensity (MFI) of 488 signal between the naïve control group and capsaicin-treated group (mean \pm SEM; $n = 5$; $*P < 0.05$ by unpaired two-tailed t -test). **c** Representative images taken by IncuCyte showing the red fluorescent intensity at different time points after incubation with pHrodo Red-labeled Zymosan; a higher magnification image with arrows indicating the Zymosan bioparticles. **d** The statistics of Zymosan phagocytosis in **c** (mean \pm SEM; $n = 8$, $*P < 0.05$, $**P < 0.01$, $***P < 0.001$ by two-way ANOVA with Tukey's multiple comparisons test). **e** The expression of TRPV1 protein was analyzed using Western blotting after incubation with siRNA-TRPV1 for 24 h. **f** The statistics of the TRPV1 protein expression in **e** (mean \pm SEM; $n = 3$; $*P < 0.05$ by unpaired one-tailed t -test). **g** Fluorescent staining of cultured microglia; cell structure was visualized using Phalloidin (green), and the Zymosan particles are in red, co-stained with Hoechst (blue); scale bar = 20 μ m; the statistics are in **k** (mean \pm SEM; $n = 8$; $*P < 0.05$ by unpaired two-tailed t -test). **h** Representative images from IncuCyte (after 24 h) showing the uptake of Zymosan by microglia. **i** The different time points of Zymosan uptake were connected as a curve and the area under the curve was calculated and compared in **j** (mean \pm SEM; $n = 8$; $*P < 0.05$ by unpaired two-tailed t -test).

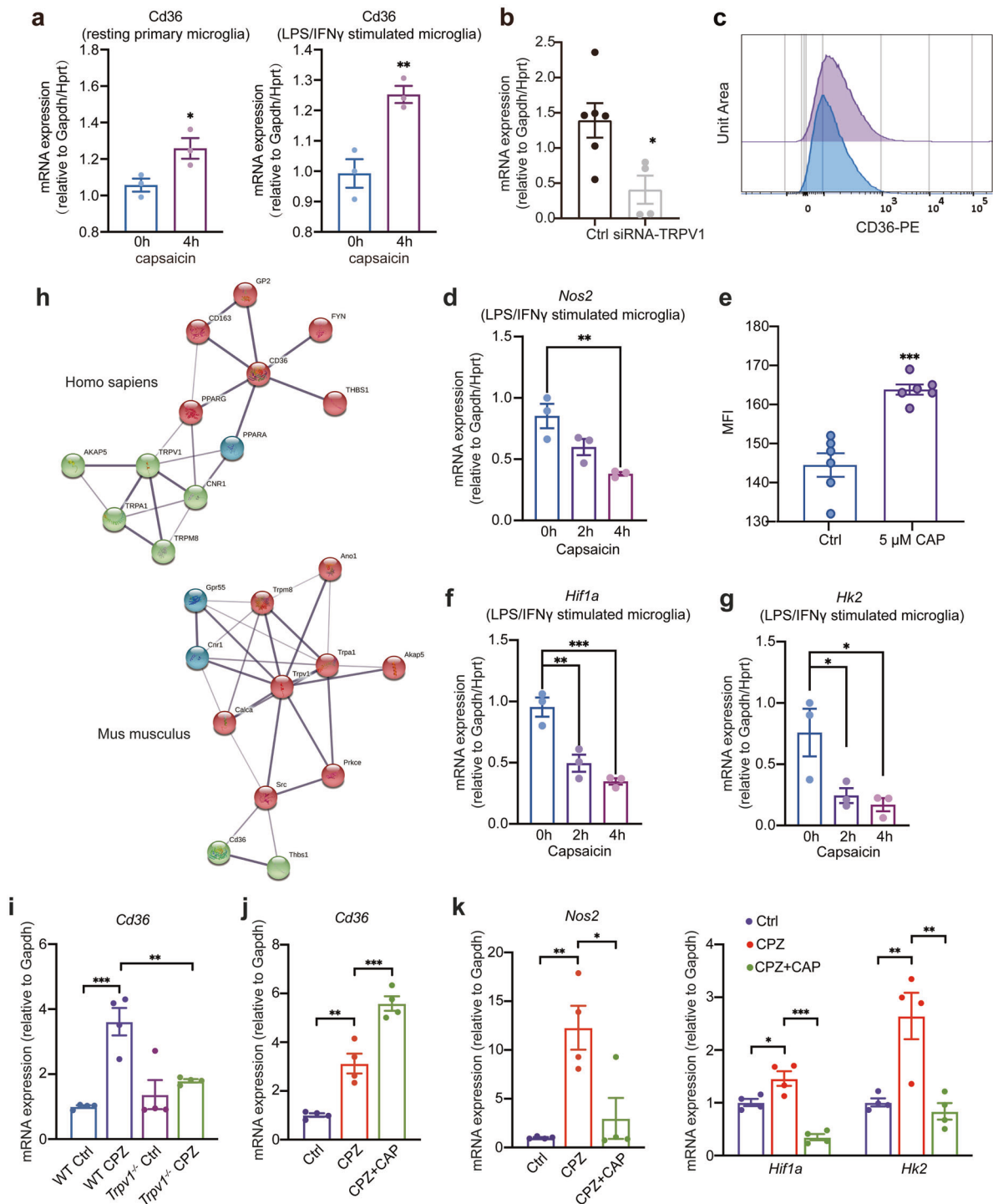


Fig. 7 The scavenger receptor CD36 is involved during TRPV1 activation. **a** mRNA expression of *Cd36* (normalized to *Gapdh* and *Hprt*) of resting and LPS/IFN γ -stimulated primary microglia treated with capsaicin for 4 h (mean \pm SEM; $n = 3$; * $P < 0.05$, ** $P < 0.01$ by unpaired two-tailed t -test). **b** mRNA expression of *Cd36* (normalized to *Gapdh* and *Hprt*) of control microglia or siRNA-TRPV1 treated microglia after 24 h (mean \pm SEM; $n = 4$ or 6; * $P < 0.05$ by unpaired two-tailed t -test). **c**, **e** Flow cytometry analysis of CD36 expression in untreated BV2 microglia or treated with 5 μ M CAP for 24 h (mean \pm SEM; $n = 6$; *** $P < 0.001$ by unpaired two-tailed t -test). **d**, **f**, and **g** mRNA expression of *Nos2* (**d**), *Hif1a* (**f**), and *Hk2* (**g**) in LPS/IFN γ -stimulated microglia treated with capsaicin for indicated hours (mean \pm SEM; $n = 3$; * $P < 0.05$, ** $P < 0.01$, *** $P < 0.001$ by one-way ANOVA with Dunnett's multiple comparisons test). **h** STRING analysis showing the close interaction between TRPV1 and CD36 in *Homo sapiens* and *Mus musculus*. **i** Gene expression analysis of *Cd36* in the corpus callosum of WT and *Trpv1*^{-/-} mice (mean \pm SEM; $n = 4$ mice for each group; *** $P < 0.001$ by two-way ANOVA with Sidak's multiple comparisons test). **j**, **k** Expression of *Cd36*, *Nos2*, *Hif1a* and *Hk2* was assessed by RT-PCR in the corpus callosum at the end of capsaicin treatment (mean \pm SEM; $n = 4$; * $P < 0.05$, ** $P < 0.01$, *** $P < 0.001$ by one-way ANOVA with Tukey's multiple comparisons test).

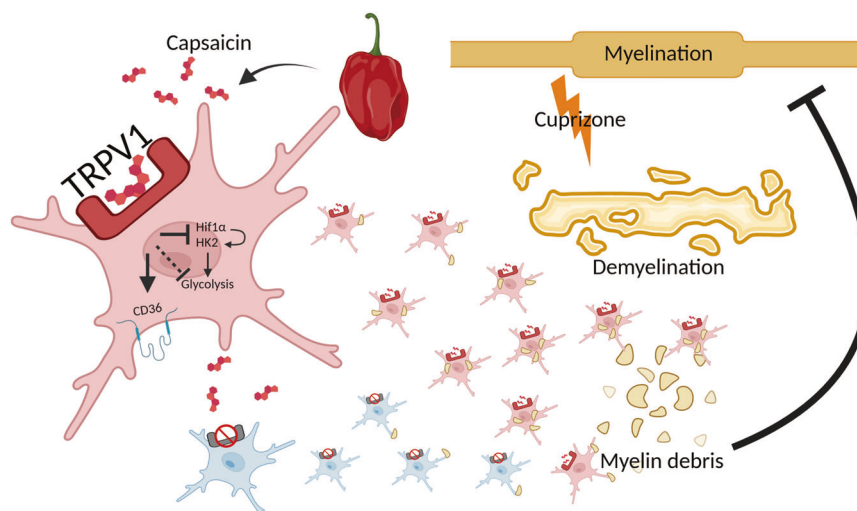


Fig. 8 A summary of the findings of the current study. In the context demyelination, TRPV1 is needed to facilitate the efficient clearance of myelin debris, a process that paves the way for subsequent remyelination. By employing loss-of-function and gain-of-function studies, we revealed that microglial function is highly affected in terms of the functional activity of TRPV1. Global activation of TRPV1 drives microglia to demyelinating sites and enhances microglial phagocytosis, whereas TRPV1-deficient microglia failed to do so. The scavenger receptor CD36 mediates the enhanced phagocytosis following TRPV1 activation in microglia, accompanied by potential metabolic shift with downregulation of glycolysis. (Illustration created with BioRender.com).

protein kinase Src reported in *Mus musculus* (Fig. 7h). CD36 is a critical regulator of fatty acid oxidation and lipid metabolism, and functions as an initiator of metabolic reprogramming shifting from glycolysis to oxidative phosphorylation in macrophages, inducing a more immunosuppressive phenotype and conferring a favorable effect on the resolution of inflammation [35]. In addition, CAP significantly downregulated the expression of the inflammatory gene *Nos2*, as well as *Hif1a* and *Hk2*, which are key genes facilitating glycolysis, indicating an underlying metabolic reprogramming (Fig. 7d, f, g). Consistent with our *in vitro* data, TRPV1 knockout in mice also downregulated the mRNA expression of *Cd36* in the CC of CPZ-treated animals (Fig. 7i). In contrast, CAP treatment increased the mRNA level of *Cd36* (Fig. 7j). We also observed that CPZ chow significantly increased the mRNA expression of *Nos2*, *Hif1a*, and *Hk2*, whereas CAP treatment suppressed the expression of these genes in the CC of CPZ-treated animals (Fig. 7k). Taken together, these data reveal that CD36 is a potential receptor that mediates the effect of CAP on microglial phagocytosis (Fig. 8).

DISCUSSION

Understanding the molecular mechanisms that regulate demyelination and facilitate myelin repair in MS is essential for the development of novel therapeutics. Previously, our group screened and identified drugs and small molecular compounds with myelin regenerating properties using *Connectivity-Map*, and capsaicin was identified as one of the top candidates [36]. TRPV1 was initially identified to be activated by capsaicin [11]. Most of the earlier work primarily studied the function of TRPV1 in sensory neurons in the context of nociception and sensory transmission. Recent studies have also demonstrated that TRPV1 is involved in many neurodegenerative and psychiatric disorders, such as Alzheimer's disease (AD), Parkinson's disease (PD), ischemia, and depression [37–40]. Herein, for the first time, we revealed the role of TRPV1 in the CPZ-induced demyelinating model. We reported that TRPV1 was upregulated in demyelinated areas following CPZ treatment. However, in other neurodegenerative contexts, such as AD, TRPV1 expression was decreased in the brain [41]. The role of TRPV1 in neurodegenerative diseases therefore needs to be further deciphered, and techniques such as single-cell RNA-

sequencing will be necessary for future studies to dissect which cells are predominantly affected.

TRPV1 activation seems to be protective in several neurological diseases. TRPV1 exerts protective effects on the autoimmune-mediated EAE mouse model of MS, in which TRPV1 regulates the release of inflammatory cytokines [23]. This is in concordance with a previous study showing that EAE mice lacking TRPV1 exhibited higher mortality at the peak of the disease [22]. TRPV1 activation by CAP significantly reduces the release of TNF and IL-6 by activated microglial cells, and MS patients with a mutation in TRPV1 that leads to reduced TRPV1 expression have higher levels of TNF in their cerebrospinal fluids [42]. Apart from MS, the potentiation of TRPV1 also correlates with the improvement of learning and memory impairment in AD mice. CAP also prevents neurons from amyloid- β ($A\beta$) peptide-induced impairment and reduces the hyperphosphorylation of tau protein in the hippocampus [43]. Moreover, CAP protects against oxidative stress-induced dopaminergic neuron loss in the MPTP mouse model of PD [44]. These studies led us to consider TRPV1 activation as a promising therapeutic strategy for neurological diseases.

Consistent with the findings in other neurological disorders, we report herein the protective role of TRPV1 in demyelinating conditions. Although TRPV1 is expressed in many brain regions, we show that TRPV1 is predominantly colocalized with microglia in regions where demyelination occurs in mouse and human. Many studies have shown that TRPV1 modulates multiple microglial functions in normal and pathological conditions [45, 46]. In line with these observations, we noted that TRPV1 deficiency reduced the recruitment of microglia into demyelinating areas, which was accompanied by an increase in accumulation of myelin debris. Our *in vitro* results confirmed that TRPV1 activation by CAP enhanced microglial migration in a concentration-dependent manner, and this effect was abolished by a TRPV1 antagonist. Our findings not only support previous studies showing the enhanced motility of microglia following CAP incubation but also provide additional *in vivo* evidence indicating that CAP treatment could help drive microglia to sites of damage [47, 48].

The efficient clearance of myelin debris following CAP treatment in the CPZ-induced demyelinating model could be a collaborative effect of both the enhanced microglial recruitment

and phagocytic functions. A study using the phytocannabinoid cannabidiol (CBD) found that CBD increased the expression of both TRPV1 and TRPV2, and enhanced the phagocytosis of both primary and BV2 microglial cells [49]. However, whether TRPV1 alone could dictate microglial phagocytosis was not addressed. In our study, we further corroborated this finding by using the more exclusive and canonical TRPV1 agonist CAP. TRPV1 activation conferred a beneficial role in the context of demyelination. Correspondingly, increased microglial recruitment in the vicinity of amyloid plaques with attenuated neuroinflammation was confirmed [50].

Many previous studies have suggested that TRPV1 is expressed in neurons with high permeability to Ca^{2+} [11]. Microglia can sense and modulate neuronal activity [51], and neurons in turn can regulate microglial function through signaling such as the CX3CL1-CX3CR1 axis [52, 53]. This mutual interaction helps maintain brain homeostasis and neural circuit regulation [51]. In our study, when capsaicin was administered systematically, neuronal functions may also be affected and thus we could not rule out the indirect effects of capsaicin on microglia via altered neuronal activities. A cell-specific capsaicin delivery strategy using myeloid cell-specific nanoparticles such as MyloGami to target macrophages/microglia may help exclude neuronal effects [54]. In addition, microglial Ca^{2+} activity is associated with multiple microglial functions, such as cytokine release [55, 56]. Over-activation of TRPV1 triggers the influx of excessive Ca^{2+} into microglia which promotes neuroinflammation [57]. However, controlled activation of microglial TRPV1 increased Ca^{2+} influx and promoted the phagocytosis of alpha-synuclein [58].

We observed an upregulation of the scavenger receptor CD36 following CAP treatment and noted the downregulation of HIF-1 α and HK2, which are key regulators of glycolysis [59], indicating a potential metabolic shift from glycolysis to oxidative phosphorylation. This is a well-characterized metabolic reprogramming that regulates the phenotypic switch of microglia toward immunosuppression. Coincidentally, a recent study also reported that the suppressed oxidative phosphorylation and aerobic glycolysis in microglia due to the activation of the mTOR-AKT-HIF-1 α pathway can be rescued by CAP [50]. PPAR γ is a member of nuclear receptor family and controls the expression of CD36 [60]. A PPAR γ agonist improves the clearance function of microglia, which is mediated by the upregulation of CD36 expression [61]. In an AD mouse model, the increased microglia phagocytic activity was mediated by the PPAR- γ /CD36 pathway [62]. TRPV1 activation was reported to increase the expression of PPAR γ in adipose tissue [63].

Further methodologies, such as RNA-sequencing, could be employed to unravel the transcription factors and key regulators that mediate the metabolic shift in microglia following CAP treatment. In addition, the findings we report herein would be further strengthened by future studies that could conditionally knockout TRPV1 in microglia.

We provide evidence that targeting TRPV1 with capsaicin appears to be a promising strategy for the treatment of CNS demyelinating diseases. Since capsaicin is the main component of chili pepper, our study may provide dietary guidance to MS patients in terms of the uptake of chili pepper in daily supplements and inspire epidemiological and clinical studies to uncover the association of chili consumption with MS incidence.

ACKNOWLEDGEMENTS

This study was supported by the National Natural Science Foundation of China (82074538, 81671597), the Innovative Research Team of High-Level Local Universities in Shanghai (2019-2023), the Shanghai Municipal Science and Technology Major Project (No. 2018SHZDZX01) and the Development Project of Shanghai Peak Disciplines-Integrated Chinese and Western Medicine. KZ was sponsored by China Scholarship Council (201700260280). We thank Meng Sun from Karolinska Institutet for the help

with setting up IncuCyte. We thank Jingdian Zhang and Shengduo Pei from Karolinska Institutet for sharing experimental reagents and materials for pilot tests.

AUTHOR CONTRIBUTIONS

We follow the International Committee of Medical Journal Editors (ICMJE) recommendations for assigning the authorship. JW designed and coordinated the experiments. JXS and KYZ performed most experiments and wrote the manuscript with assistance from YMW, HS, IBC, MZZ and DJW. MZZ, ZFZ, XQZ and QYZ were involved in behavioral tests. RAH and JW supervised the study with scientific input (with contributions from YMW, SW and YF). All the authors reviewed and revised the manuscript.

ADDITIONAL INFORMATION

Supplementary information The online version contains supplementary material available at <https://doi.org/10.1038/s41401-022-01000-7>.

Competing interests: The authors declare no competing interests.

REFERENCES

1. Stadelmann C, Timmler S, Barrantes-Freer A, Simons M. Myelin in the Central nervous system: structure, function, and pathology. *Physiol Rev*. 2019;99:1381–431.
2. Franklin RJM, Ffrench-Constant C. Regenerating CNS myelin—from mechanisms to experimental medicines. *Nat Rev Neurosci*. 2017;18:753–69.
3. Lubetzki C, Zalc B, Williams A, Stadelmann C, Stankoff B. Remyelination in multiple sclerosis: from basic science to clinical translation. *Lancet Neurol*. 2020;19:678–88.
4. Reich DS, Lucchinetti CF, Calabresi PA. Multiple sclerosis. *N Engl J Med*. 2018;378:169–80.
5. Faissner S, Plemel JR, Gold R, Yong VW. Progressive multiple sclerosis: from pathophysiology to therapeutic strategies. *Nat Rev Drug Discov*. 2019;18:905–22.
6. Prinz M, Jung S, Priller J. Microglia biology: one century of evolving concepts. *Cell*. 2019;179:292–311.
7. Voet S, Prinz M, van Loo G. Microglia in central nervous system inflammation and multiple sclerosis pathology. *Trends Mol Med*. 2019;25:112–23.
8. International Multiple Sclerosis Genetics Consortium. Multiple sclerosis genomic map implicates peripheral immune cells and microglia in susceptibility. *Science*. 2019;365:eaav7188.
9. Olsson T, Barcellos LF, Alfredsson L. Interactions between genetic, lifestyle and environmental risk factors for multiple sclerosis. *Nat Rev Neurol*. 2017;13:25–36.
10. Moran MM, McAlexander MA, Biró T, Szallasi A. Transient receptor potential channels as therapeutic targets. *Nat Rev Drug Discov*. 2011;10:601–20.
11. Caterina MJ, Schumacher MA, Tominaga M, Rosen TA, Levine JD, Julius D. The capsaicin receptor: a heat-activated ion channel in the pain pathway. *Nature*. 1997;389:816–24.
12. Szallasi A, Blumberg PM. Vanilloid (Capsaicin) receptors and mechanisms. *Pharmacol Rev*. 1999;51:159–212.
13. Sasamura T, Sasaki M, Tohda C, Kuraishi Y. Existence of capsaicin-sensitive glutamatergic terminals in rat hypothalamus. *Neuroreport*. 1998;9:2045–8.
14. Mezey E, Tóth ZE, Cortright DN, Arzubi MK, Krause JE, Elde R, et al. Distribution of mRNA for vanilloid receptor subtype 1 (VR1), and VR1-like immunoreactivity, in the central nervous system of the rat and human. *Proc Natl Acad Sci USA*. 2000;97:3655–60.
15. Roberts JC, Davis JB, Benham CD. [3H]Resiniferatoxin autoradiography in the CNS of wild-type and TRPV1 null mice defines TRPV1 (VR-1) protein distribution. *Brain Res*. 2004;995:176–83.
16. Tóth A, Boczán J, Kedei N, Lizanecz E, Bagi Z, Papp Z, et al. Expression and distribution of vanilloid receptor 1 (TRPV1) in the adult rat brain. *Brain Res Mol Brain Res*. 2005;135:162–8.
17. Cristino L, de Petrocellis L, Pryce G, Baker D, Guglielmotti V, Di Marzo V. Immunohistochemical localization of cannabinoid type 1 and vanilloid transient receptor potential vanilloid type 1 receptors in the mouse brain. *Neuroscience*. 2006;139:1405–15.
18. Edwards JG. TRPV1 in the central nervous system: synaptic plasticity, function, and pharmacological implications. *Prog Drug Res*. 2014;68:77–104.
19. Kong WL, Peng YY, Peng BW. Modulation of neuroinflammation: role and therapeutic potential of TRPV1 in the neuro-immune axis. *Brain Behav Immun*. 2017;64:354–66.
20. Ramirez-Barrantes R, Cordova C, Poblete H, Muñoz P, Marchant I, Wianny F, et al. Perspectives of TRPV1 function on the neurogenesis and neural plasticity. *Neural Plast*. 2016;2016:1568145.

21. Huang WX, Yu F, Sanchez RM, Liu YQ, Min JW, Hu JJ, et al. TRPV1 promotes repetitive febrile seizures by pro-inflammatory cytokines in immature brain. *Brain Behav Immun*. 2015;48:68–77.
22. Musumeci G, Grasselli G, Rossi S, De Chiara V, Musella A, Motta C, et al. Transient receptor potential vanilloid 1 channels modulate the synaptic effects of TNF- α and of IL-1 β in experimental autoimmune encephalomyelitis. *Neurobiol Dis*. 2011;43:669–77.
23. Tsuji F, Murai M, Oki K, Seki I, Ueda K, Inoue H, et al. Transient receptor potential vanilloid 1 agonists as candidates for anti-inflammatory and immunomodulatory agents. *Eur J Pharmacol*. 2010;627:332–9.
24. Barclay W, Shinohara ML. Inflammasome activation in multiple sclerosis and experimental autoimmune encephalomyelitis (EAE). *Brain Pathol*. 2017;27:213–9.
25. Zhu K, Sun J, Kang Z, Zou Z, Wu G, Wang J. Electroacupuncture promotes remyelination after cuprizone treatment by enhancing myelin debris clearance. *Front Neurosci*. 2016;10:613.
26. Polman CH, Reingold SC, Edan G, Filippi M, Hartung HP, Kappos L, et al. Diagnostic criteria for multiple sclerosis: 2005 revisions to the “McDonald Criteria”. *Ann Neurol*. 2005;58:840–6.
27. Martins D, Tavares I, Morgado C. “Hotheaded”: the role OF TRPV1 in brain functions. *Neuropharmacology*. 2014;85:151–7.
28. Doly S, Fischer J, Salio C, Conrath M. The vanilloid receptor-1 is expressed in rat spinal dorsal horn astrocytes. *Neurosci Lett*. 2004;357:123–6.
29. Marrone MC, Morabito A, Giustizieri M, Chiurciu V, Leuti A, Mattioli M, et al. TRPV1 channels are critical brain inflammation detectors and neuropathic pain biomarkers in mice. *Nat Commun*. 2017;8:15292.
30. Lloyd AF, Miron VE. The pro-remyelination properties of microglia in the central nervous system. *Nat Rev Neurol*. 2019;15:447–58.
31. Skripuletz T, Hackstette D, Bauer K, Gudi V, Pul R, Voss E, et al. Astrocytes regulate myelin clearance through recruitment of microglia during cuprizone-induced demyelination. *Brain*. 2013;136:147–67.
32. Lampron A, Laroche A, Laflamme N, Préfontaine P, Plante MM, Sánchez MG, et al. Inefficient clearance of myelin debris by microglia impairs remyelinating processes. *J Exp Med*. 2015;212:481–95.
33. Choi JJ, Wang S, Tung YS, Morrison B 3rd, Konofagou EE. Molecules of various pharmacologically-relevant sizes can cross the ultrasound-induced blood-brain barrier opening in vivo. *Ultrasound Med Biol*. 2010;36:58–67.
34. Zhu Z, Zheng L, Li Y, Huang T, Chao YC, Pan L, et al. Potential immunotherapeutic targets on myeloid cells for neurovascular repair after ischemic stroke. *Front Neurosci*. 2019;13:758.
35. Woo MS, Yang J, Beltran C, Cho S. Cell surface CD36 protein in monocyte/macrophage contributes to phagocytosis during the resolution phase of ischemic stroke in mice. *J Biol Chem*. 2016;291:23654–61.
36. Zhu K, Sun J, Kang Z, Zou Z, Wu X, Wang Y, et al. Repurposing of omeprazole for oligodendrocyte differentiation and remyelination. *Brain Res*. 2019;1710:33–42.
37. Balleza-Tapia H, Crux S, Andrade-Talavera Y, Dolz-Gaiton P, Papadia D, Chen G, et al. TrpV1 receptor activation rescues neuronal function and network gamma oscillations from A β -induced impairment in mouse hippocampus in vitro. *Elife*. 2018;7:e37703.
38. Zhao Z, Wang J, Wang L, Yao X, Liu Y, Li Y, et al. Capsaicin protects against oxidative insults and alleviates behavioral deficits in rats with 6-OHDA-induced Parkinson’s disease via activation of TRPV1. *Neurochem Res*. 2017;42:3431–8.
39. Cao Z, Balasubramanian A, Marrelli SP. Pharmacologically induced hypothermia via TRPV1 channel agonism provides neuroprotection following ischemic stroke when initiated 90 min after reperfusion. *Am J Physiol Regul Integr Comp Physiol*. 2014;306:R149–56.
40. Patel S, Hill MN, Cheer JF, Wotjak CT, Holmes A. The endocannabinoid system as a target for novel anxiolytic drugs. *Neurosci Biobehav Rev*. 2017;76:56–66.
41. Du Y, Fu M, Huang Z, Tian X, Li J, Pang Y, et al. TRPV1 activation alleviates cognitive and synaptic plasticity impairments through inhibiting AMPAR endocytosis in APP23/PS45 mouse model of Alzheimer’s disease. *Aging Cell*. 2020;19:e13113.
42. Stampanoni Bassi M, Gentile A, Iezzi E, Zagaglia S, Musella A, Simonelli I, et al. Transient receptor potential vanilloid 1 modulates central inflammation in multiple sclerosis. *Front Neurol*. 2019;10:30.
43. Xu W, Liu J, Ma D, Yuan G, Lu Y, Yang Y. Capsaicin reduces Alzheimer-associated tau changes in the hippocampus of type 2 diabetes rats. *PLoS ONE*. 2017;12:e0172477.
44. Chung YC, Baek JY, Kim SR, Ko HW, Bok E, Shin WH, et al. Capsaicin prevents degeneration of dopamine neurons by inhibiting glial activation and oxidative stress in the MPTP model of Parkinson’s disease. *Exp Mol Med*. 2017;49:e298.
45. Kim SR, Kim SU, Oh U, Jin BK. Transient receptor potential vanilloid subtype 1 mediates microglial cell death in vivo and in vitro via Ca²⁺-mediated mitochondrial damage and cytochrome c release. *J Immunol*. 2006;177:4322–9.
46. Schilling T, Eder C. Importance of the non-selective cation channel TRPV1 for microglial reactive oxygen species generation. *J Neuroimmunol*. 2009;216:118–21.
47. Miyake T, Shirakawa H, Nakagawa T, Kaneko S. Activation of mitochondrial transient receptor potential vanilloid 1 channel contributes to microglial migration. *Glia*. 2015;63:1870–82.
48. Kong W, Wang X, Yang X, Huang W, Han S, Yin J, et al. Activation of TRPV1 contributes to recurrent febrile seizures via inhibiting the microglial M2 phenotype in the immature brain. *Front Cell Neurosci*. 2019;13:442.
49. Hassan S, Eldeeb K, Millns PJ, Bennett AJ, Alexander SP, Kendall DA. Cannabidiol enhances microglial phagocytosis via transient receptor potential (TRP) channel activation. *Br J Pharmacol*. 2014;171:2426–39.
50. Lu J, Zhou W, Dou F, Wang C, Yu Z. TRPV1 sustains microglial metabolic reprogramming in Alzheimer’s disease. *EMBO Rep*. 2021;22:e52013.
51. Umpierre AD, Wu LJ. How microglia sense and regulate neuronal activity. *Glia*. 2021;69:1637–53.
52. Chen X, Jiang M, Li H, Wang Y, Shen H, Li X, et al. CX3CL1/CX3CR1 axis attenuates early brain injury via promoting the delivery of exosomal microRNA-124 from neuron to microglia after subarachnoid hemorrhage. *J Neuroinflammation*. 2020;17:209.
53. Nguyen PT, Dorman LC, Pan S, Vainchtein ID, Han RT, Nakao-Inoue H, et al. Microglial remodeling of the extracellular matrix promotes synapse plasticity. *Cell*. 2020;182:388–403.
54. Zhu K, Wang Y, Sarlus H, Geng K, Nutma E, Sun J, et al. Myeloid cell-specific topoisomerase 1 inhibition using DNA origami mitigates neuroinflammation. *EMBO Rep*. 2022;23:e54499.
55. Umpierre AD, Bystrom LL, Ying Y, Liu YU, Worrell G, Wu LJ. Microglial calcium signaling is attuned to neuronal activity in awake mice. *Elife*. 2020;9:e56502.
56. Yi MH, Liu YU, Umpierre AD, Chen T, Ying Y, Zheng J, et al. Optogenetic activation of spinal microglia triggers chronic pain in mice. *PLoS Biol*. 2021;19:e3001154.
57. Zhang Y, Hou B, Liang P, Lu X, Wu Y, Zhang X, et al. TRPV1 channel mediates NLRP3 inflammasome-dependent neuroinflammation in microglia. *Cell Death Dis*. 2021;12:1159.
58. Yuan J, Liu H, Zhang H, Wang T, Zheng Q, Li Z. Controlled activation of TRPV1 channels on microglia to boost their autophagy for clearance of alpha-synuclein and enhance therapy of Parkinson’s disease. *Adv Mater*. 2022;34:e2108435.
59. Gordan JD, Thompson CB, Simon MC. HIF and c-Myc: sibling rivals for control of cancer cell metabolism and proliferation. *Cancer Cell*. 2007;12:108–13.
60. Mikkelsen TS, Xu Z, Zhang X, Wang L, Gimble JM, Lander ES, et al. Comparative epigenomic analysis of murine and human adipogenesis. *Cell*. 2010;143:156–69.
61. Yamanaka M, Ishikawa T, Griep A, Axt D, Kummer MP, Heneka MT. PPAR γ /RXR α -induced and CD36-mediated microglial amyloid- β phagocytosis results in cognitive improvement in amyloid precursor protein/presenilin 1 mice. *J Neurosci*. 2012;32:17321–31.
62. Medrano-Jiménez E, Jiménez-Ferrer Carrillo I, Pedraza-Escalona M, Ramírez-Serrano CE, Álvarez-Arellano L, Cortés-Mendoza J, et al. Malva parviflora extract ameliorates the deleterious effects of a high fat diet on the cognitive deficit in a mouse model of Alzheimer’s disease by restoring microglial function via a PPAR- γ -dependent mechanism. *J Neuroinflammation*. 2019;16:143.
63. Krishnan V, Baskaran P, Thyagarajan B. Troglitazone activates TRPV1 and causes deacetylation of PPAR γ in 3T3-L1 cells. *Biochim Biophys Acta Mol Basis Dis*. 2019;1865:445–53.

Springer Nature or its licensor holds exclusive rights to this article under a publishing agreement with the author(s) or other rightsholder(s); author self-archiving of the accepted manuscript version of this article is solely governed by the terms of such publishing agreement and applicable law.